Scientific Research Publishing

Open Journal of Radiology, 2020, 10, 57-68
https://www.scirp.org/journal/ojrad
ISSN Online: 2164-3032
ISSN Print: 2164-3024

Pediatric Application of Dynamic Contrast-Enhanced MR Imaging (DCE-MR) in the Management of Extra-Cranial Tumor: Experience in Routine Clinical Practice

Wendy Wai-Man Lam[1*], Daniel Cheuk[2], Godfrey Chi-Fung Chan[2]

[1]Department of Radiology, Queen Mary Hospital, Hong Kong SAR, China
[2]Department of Paediatrics & Adolescent Medicine, The University of Hong Kong, Hong Kong SAR, China
Email: *lamwendy60@yahoo.com.hk

How to cite this paper: Lam, W.W.-M., Cheuk, D. and Chan, G.C.-F. (2020) Pediatric Application of Dynamic Contrast-Enhanced MR Imaging (DCE-MR) in the Management of Extra-Cranial Tumor: Experience in Routine Clinical Practice. *Open Journal of Radiology*, **10**, 57-68.
https://doi.org/10.4236/ojrad.2020.102007

Received: May 7, 2020
Accepted: May 29, 2020
Published: June 1, 2020

Copyright © 2020 by author(s) and Scientific Research Publishing Inc.
This work is licensed under the Creative Commons Attribution International License (CC BY 4.0).
http://creativecommons.org/licenses/by/4.0/

Open Access

Abstract

Background: Dynamic contrast-enhanced MR imaging (DCE-MR) is becoming a widely accepted complementary method for diagnosing breast cancer and other cancers in adults. It is useful to predict tumor response to anticancer therapy and monitor the tumor response to the therapy. This form of imaging techniques has not been adequately explored in pediatric oncology patients. **Objective:** To determine the potential role of dynamic contrast-enhanced MR imaging (DCE-MR) in the diagnosis and treatment response monitoring of childhood and young adult extra-cranial tumors in routine clinical setting. **Methods:** Children with suspected extra-cranial solid tumors, including newly diagnosed or follow-up cases of confirmed tumors, were recruited. DCE-MR was performed with intravenous injection of 0.1 mmol/kg contrast. The enhancement time curves were plotted and the enhancement patterns were categorized into type 1, 2 and 3 curves. Enhancement curve patterns and maximal enhancement intensity were compared with types of tumor in newly diagnosed cases. The preoperative percentiles of inactive area on the colour map were compared with the necrotic areas on histologic sections of the resected specimens in follow-up cases. Pearson Chi-square test and Unpaired two-sample t-test were used for statistical analysis. **Results:** There were 36 patients, involving 28 malignant and 8 benign cases. There were 14 type 3 curves, (all of them were malignant tumors), 6 type 2 curves and 16 type 1 curves. All the benign cases (n = 8) demonstrated type 1 curve (accuracy & negative predictive value = 100%). All the malignant cases after treatment showed type 2 or 1 curve. For those cases with operation done afterwards, the extent of tumor necrosis was correlated closely with pathology

findings (accuracy = 93.3%). **Conclusion:** Type 1 curve was a good predictor of benign lesion. DEC-MR may have a role to play in the monitoring of the progress of treatment and extent of tumor necrosis.

Keywords

MR, DCE-MR, Dynamic Contrast MR, Tumor, Children, Pediatric

1. Introduction

Radiologists are often required to provide information on clinical questions such as diagnosis, staging, treatment response, and detection of either residual or recurrent lesions in oncology patients. MRI is a useful tool in assisting the diagnosis, defining the extent of diseases and monitoring the response to therapy. Dynamic contrast-enhanced MR imaging (DCE-MR) is becoming a widely accepted complementary method for diagnosing breast cancer and other cancers in adults [1] [2]. It can help to monitor the effect of anti-angiogenic treatment response [3] [4]. But this form of imaging techniques have not been adequately explored in pediatric oncology patients. There were not many applications in pediatric extra-cranial tumours.

Previous studies using DCE-MR demonstrated that malignant tumors usually showed faster and higher levels of enhancement than normal tissue [2]. This enhancement characteristic indicated that malignant tumors have increased vascularity and endothelial permeability to the contrast molecules than that of normal or less aggressive malignant tissues. Weidner *et al.* [4] demonstrated that in many tumors such as breast, lung, prostate, and head and neck cancer, the measurements of microvascular density made on histopathological samples correlated closely with clinical stage and acted as an independent prognostic factor of considerable sensitivity. The relationship could be due to the rapid tumor growth which could only be supported by highly active angiogenesis. The more aggressive tumors were therefore associated with higher angiogenesis-related microvasculature abnormalities. On the basis of this histopathological evidence it had been suggested that DCE-MR might be able to provide additional independent indices of angiogenic activity and therefore acted as a prognostic indicator in a broad range of tumor types. DCE-MR time intensity curve (TIC) patterns are categorized to three types: type 1, persistently enhancing (progressive), which is suggestive of less angiogenic; type 2, plateau type, which has an intermediate probability for malignancy; and type 3, washout type, which is indicative of malignancy with a lot of angiogenesis [2] [5]. DCE-MR is also useful to predict tumor response to anticancer therapy and monitoring the tumor response to the therapy [6] [7] [8].

This study tried to explore the possible role of DCE-MR in the diagnosis and treatment response monitoring of childhood and young adult extra-cranial tu-

mors in routine clinical setting.

2. Materials and Methods

2.1. Subjects

This was a prospective study. From 2014 to 2016, all children and young adults younger than 20 years old attending the oncology clinic with suspected extracranial tumors were recruited for MR examinations. All examinations were done in the Department of Radiology in our local institution, involved patients including newly diagnosed or follow-up cases of malignant tumors. Follow-up cases were those who underwent neoadjuvant chemo- or radiotherapy. This study was approved by the Institutional Review Board in our hospital. Informed consent was obtained from the parents. Newly diagnosed cases with no diagnostic biopsy and follow-up cases with no post-treatment operation were excluded.

2.2. MR Imaging

MR imaging was performed using a 1.5T superconducting whole-body imager (GE Signa Horizon Echospeed, Milwaukee). Conventional MR examinations including T1W and T2W images were performed and dynamic axial scan was then conducted using three-dimensional FSPGR sequences (TR: 200 - 300 ms, TE: 2 ms, flip angle:70 degrees, slice thickness: 5-10mm depending on the size of tumour, imaging matrix: 256 × 128 − 160, No. of excitation: 1) after intravenous injection of 0.1 mmol/kg Gadolinium contrast. The size of the needle was 22 Gauge with an injection rate about 2 ml/second. For very small children, we used hand injection. The image acquisition time of each phase was 15 s - 30 s depending on the number of slices. Images were taken immediately after the injection and continued up to 5 minutes.

2.3. MRI Quantitative Analysis

Post data analysis was conducted using Functool software. A region of interest (ROI) was placed in the lumen of the nearest large artery to evaluate the arterial input function. Consecutively, perfusion and tissue-blood ratio were calculated and colour mapping was generated. ROIs were drawn around its highest vascularised and different parts of the tumour or mass according to the different distribution on the colour map. Additional ROIs were also placed at adjacent normal muscle or tissue for comparison. Signal intensity (SI) values were measured in operator-defined ROIs. The SI values derived from the ROIs were plotted against time as time intensity curve (TIC). TIC was plotted and the enhancement patterns were divided into type 1, 2 and 3 curves. Type 1 curve showed a gradual continual persistent rise after the arrival of the arterial bolus (progressive). Type 2 curve showed relatively rapid increase after the arrival of the arterial bolus and then became plateau or static. Under Type 3 curve, TIC demonstrated a sharp rise of contrast enhancement in the tumor after the arrival of the arterial bolus and then followed by a steeper wash-out (**Figure 1**).

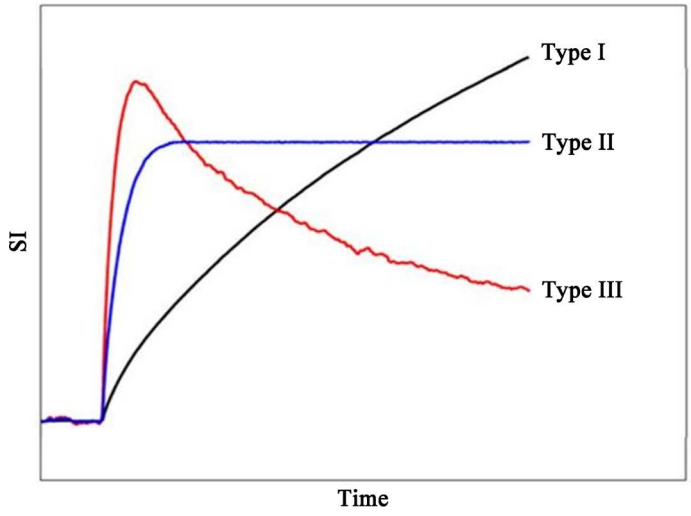

Figure 1. Schematic diagram showing different patterns of curves: Type 1 (black), Type 2 (blue) and Type 3 (red).

The curve patterns and maximal enhancement intensity (SI_{max}) were correlated with the type of tumours (pathological confirmed) in first diagnosed cases.

For those follow-up cases of tumors after neoadjuvant chemo or radiotherapy, MR was performed within a few days before the operation. The tumour inactive area was defined by the area of lack of signal changes on the color map and TIC curve. The percentile of tumour inactive area was defined as the ratio between inactive area and the overall tumour volume. The preoperative percentile of inactive area on the colour map was compared with the necrotic areas on histologic sections of the resected specimens.

2.4. Statistical Analysis

Statistical analyses were performed using SPSS version 15.0. Pearson Chi-square test

$$\chi^2 = \sum \frac{(O\_E)^2}{E} \tag{1}$$

was used to test the dependence of types of tumor upon types of curve. The observed frequency (O) and the expected frequency (E) for each type of curves were used to calculate the χ^2 value.

Unpaired two-sample t-test

$$T = \frac{x1\_x2}{\sqrt{\frac{s1^2}{N1} + \frac{s2^2}{N2})}} \tag{2}$$

was used to analyse the relationship between type of tumor and the SI_{max} ($x1$ = SI_{max} mean of benign tumor, $x2$ = SI_{max} mean of malignant tumor, $s1$ = SD of benign tumor, $s2$ = SD of malignant tumor, $N1$ = samples size of benign tumor, $N2$ = samples size of malignant tumor) The calculated T statistic value was used to decide if there is a significant difference in the SI_{max} between the benign and

malignant tumor.

A p-value < 0.05 (two-tail) was considered to be statistically significant.

3. Results

A total of 36 studies (M = 29, F = 7) were performed, with average age 9.87 yrs old and with ages ranging from 1 month to 20 years old. There were 28 malignant cases and 8 benign cases (Table 1).

3.1. Newly Diagnosed Cases

There were 21 newly diagnosed cases including 3 intra-abdominal, retroperitoneal

Table 1. Demography of all patients including newly diagnosed and follow-up cases.

Type of Tumor	Sex	Age (Years)	Follow-up with repeat study
Chronic granulomatous tissue	M	4	No
Osteomyelitis	M	1.6	No
Stress fracture	F	9	No
Neurofibroma	M	20	No
Neurofibroma	M	2.8	No
Thigh Fat necrosis	M	10	No
Ganglioneuroma	M	0.7	No
Fibromuscular tissue	F	7	No
Osteogenic sarcoma	M	10	Yes
Pelvic neuroblastoma	M	0.2	Yes
Neuroblastoma	F	3	Yes
Arm pPNET	M	15	Yes
Osteogenic sarcoma	F	6	Yes
Osteogenic sarcoma	M	13	Yes
Langerhans cell of Histiocytosis	M	4	No
Neuroblastoma	M	4	Yes
Paraspinal PNET	M	14	Yes
Paraspinal PNET	M	15	Yes
Osteogenic sarcoma	M	14	Yes
Carcinoma pancreas	M	18	No
Rhabdomysarcoma	F	6	No
Ewing sarcoma	M	20	Yes*
Neuroblastoma	M	8	Yes*
Osteogenic sarcoma	M	12	Yes*
Neuroblastoma	M	8	Yes*
Neuroblastoma	M	3	Yes*

*Follow-up cases only.

or pelvic neuroblastoma; 4 distal femur or fibular osteogenic sarcoma, 1 Langerhans cell Histiocytosis in femur, 1 upper limb and 2 paraspinal peripheral primitive neuroectodermal tumour (pPNET), 1 parapharyngeal rhabomyosarcoma. They all showed type 3 curve at the most active area (Figure 2).

Their mean SI_{max} was about 712 (range = 200 - 1200). There was 1 case of carcinoma of pancreas which showed a type 2 curve. The SI_{max} was 200. There were 8 benign cases (fibular osteomyelitis = 1, jaw chronic granulomatous tissue = 1, paraspinal ganglioneuroma = 2, submandibular fibromuscular tissue = 1, submandibular neurofibroma = 1, fracture tibia = 1, thigh fat necrosis = 1). They all demonstrated type 1 curve patterns and the mean SI_{max} was about 350 (range = 200 - 400). There was statistical significance ($p = 0.0391$, <0.05) in the correlation of type 3 curve with malignant tumor and type 1 curve with benign tumor by using chi-square test. By applying the unpaired two-sample t-test, the means of the SI_{max} had significant difference ($p < 0.05$) between the benign (mean = 333) and malignant (mean = 572) groups (Figure 3). The negative predictive value of type 1 curve (Figure 4) was 100%.

3.2. Post-Treatment Cases

There were 15 post-chemotherapy cases and 16 follow up scans (neuroblastoma = 6, pPNET = 3, osteogenic sarcoma = 5, pelvis Ewing sarcoma = 1). The maximal enhancement intensity (SI_{max}) of all cases was about 300 - 400 on the follow up scans. Due to the different patterns of enhancement in different tumours and different patients, we compared the enhancement patterns within the same patients.

Among 6 cases of intra-abdominal, retroperitoneal or pelvic neuroblastoma, there were 2 type 1 curves and 4 type 2 curves after treatment. They all showed greater than 50% central necrosis according to the color map. Among 3 pPNET,

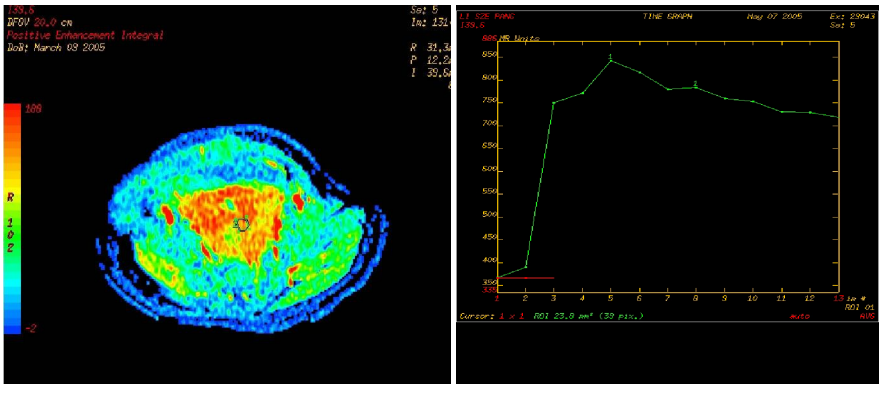

(a) (b)

Figure 2. 3-year-old boy with Pelvic Neuroblastoma. DCE-MR axial image before chemotherapy. (a) Axial Color image showing area of maximal enhancement (Yellow to red). No significant non-active area seen. Region of interest was placed at the hypervascular area and showed (b) Type 3 curve, a sharp rise followed by a steeper wash-out. The horizontal red line is arrival time of the arterial bolus. Maximal enhancement intensity (SI_{max}) was 850.

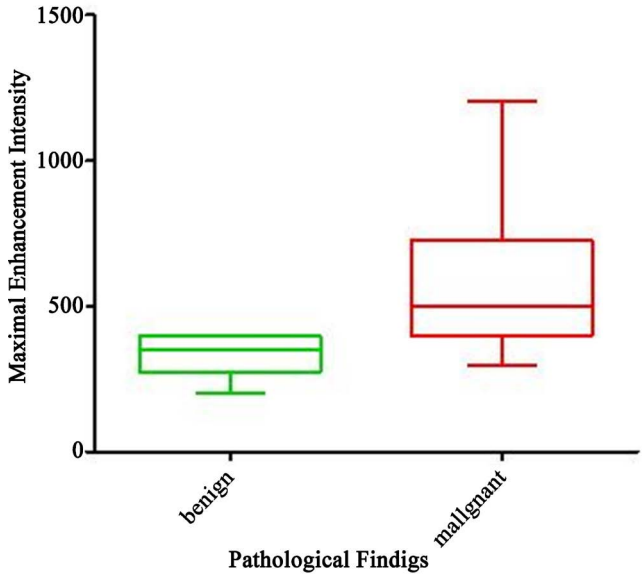

Figure 3. The pathological findings versus maximal enhancement intensity graph showing benign tumors had lower maximal enhancement intensity (SI_{max}) compared to malignant tumors.

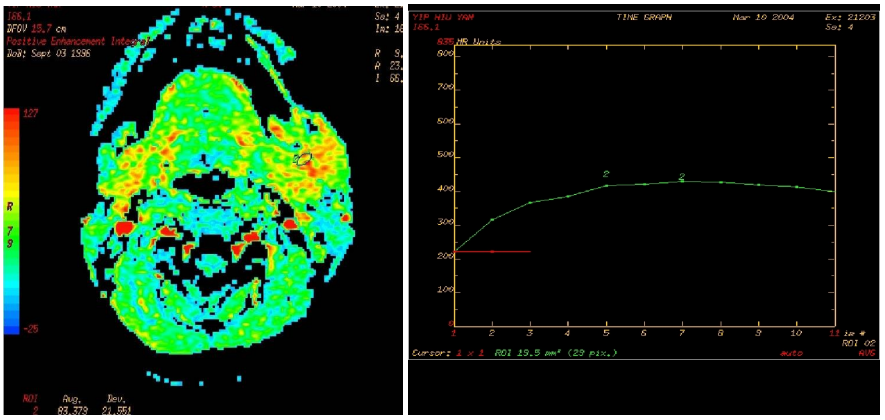

(a) (b)

Figure 4. 7-year-old girl with benign fibromuscular tumor of left submandibular gland. DCE-MR axial images of the tumor. (a) Axial Color image showing area of maximal enhancement (Yellow) and (b) type 1 curve. The horizontal red line is arrival time of the arterial bolus. Maximal enhancement intensity (SI_{max}) was 400.

one arm pPNET case showed heterogeneous peripheral type 3 curve with center type 1 - 2 curve during the first scan, but type 1 - 2 curve on the second follow-up scan irrespective of the increasing size of the tumor. Peripheral type 3 curve with center type 1 - 2 curve with area of necrosis was noted on the third scan. It was found that an enlarged axillary lymph node compressed onto the axillary vessels during the second scan and it reduced in size during the third scan. The other 2 paraspinal pPNET cases showed type 1 curves with greater than 90% necrosis on the follow-up. The pelvic Ewing sarcoma showed type 1 curve with greater than 90% central necrosis. For the 5 cases of osteogenic sarcoma, 4 cases showed type 1 curve with greater than 90% central necrosis and 1

case showed peripheral type 3 curve with 50% central necrosis. Surgical resections were performed after chemotherapy and the percentage of central necrosis was correlated well with the pathology findings (accuracy = 93.3%, n = 14/15) (Figure 5, Figure 6, Table 2).

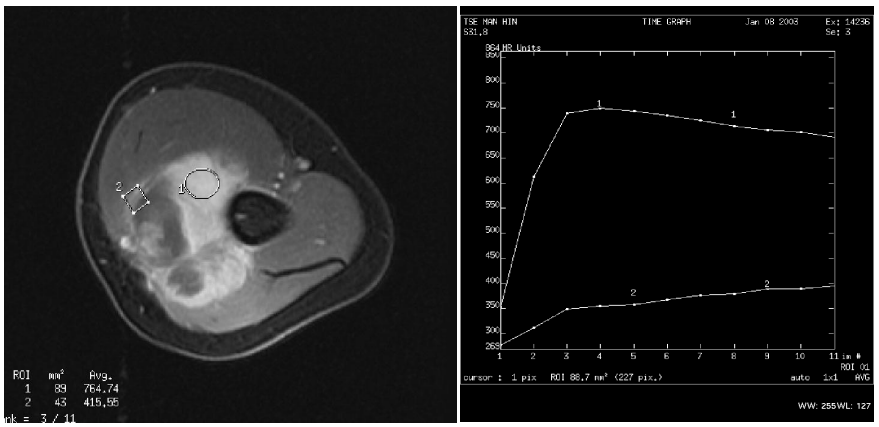

(a) (b)

Figure 5. 15-year-old boy with arm peripheral primitive neuroectodermal tumor (pPNET). DCE-MR axial image before chemotherapy. (a) Axial image showing region of interest at hypervascular region (No 1) and near necrotic area (No 2) (38%) (b) type 3 curve at hypervascular region (No 1) (SI_{max} 750) and type 1 curve at necrotic area (No 2) Maximal signal intensity (SI_{max}) was 350.

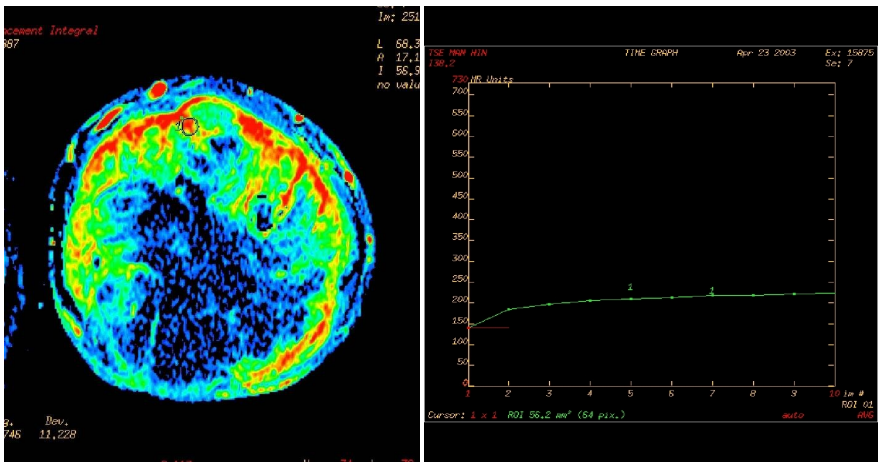

(a) (b)

Figure 6. 15-year-old boy with arm peripheral primitive neuroectodermal tumor (pPNET). DCE-MR axial images at the third follow-up before surgery. (a) Axial Color image showing hypervascular region (red) and (b) type 2 curve at most active area (SI_{max} 380).

4. Discussion

In our study, most of the tumors were peripheral solid tumors of musculoskeletal or blastoma origins. The initial result was encouraging. We found that type 3 curve pattern applied to many newly diagnosed malignant extra-cranial solid tumors irrespective of their location, such as Ewing sarcoma, pPNET, Langerhans

Table 2. Comparison between pre- and post-treatment follow-up DCE-MRI in 15 patients.

Type of Tumor	Pre-treatment Curve type	Post-treatment Curve type	Pre-treatment Mean SI_{max}	Post-treatment Mean SI_{max}	Pre-treatment Mean percentile of not active area	Post-treatment Mean Percentile of not active area	Post-treatment Pathology percentile of necrotic area (a)
Neurobststoma	3 (n = 6)	1 (n = 2)	700	350 (periphery)	0%	50%	50%
		2 (n = 4)	700	350 (periphery)	0%	50%	50%
Arm PNET	3 (n = 1)	Periphery Type 3 & central type 1/2 (n = 1)	750 (periphery)	380 (periphery)	38%	70%	50%
Spinal PNET	3 (n = 2)	1 (n = 2)	400	300 (periphery)	20%	90%	90%
Pelvic Ewing sarcoma	3 (n = 1)	1 (n = 1)	700	300 (periphery)	0%	90%	90%
Osteogenic sarcoma	Periphery type 3 & central 1/2 (n = 5)	Periphery type 3 & central 1/2 (n = 5)	1050 (periphery)	600 (periphery)	48% (n = 4) 17% (n = 1)	90% (n = 4) 50% (n = 1)	90% (n = 4) 50% (n = 1)

a. Correlation with the pathology findings accuracy = 93.3% (n = 14/15).

cell of Histiocytosis, rhabomyosarcoma, intra-abdominal and pelvic neuroblastoma. All of our first diagnosed osteogenic sarcoma showed type 3 malignant curve patterns at the peripheral active area.

The Ewing's family tumors including Ewing's sarcoma and peripheral primitive neuroectodermal tumor (pPNET) are the second most common malignant osseous tumors in children and adolescents. The pre-operative chemotherapy response by histological analysis is of prognostic value. The standard threshold separating good responders from poor is greater than 90% necrosis (less than 10% viable tumor) [9]. Neuroblastoma and other solid tumors are similar to other muscular tumors and response to chemotherapy is also considered good if there is significant tumor necrosis. Our study demonstrated the usefulness of DEC-MR in the prediction of different degree of necrosis or response to treatment on the follow-up scans. The degree of necrosis correlated well with the pathology findings except for 1 case of pPNET in the arm. This was probably due to an enlarged axillary lymph node compressing on axillary vessels, thus impairing the flow dynamic of TIC.

Osteogenic sarcoma often requires biopsy for definitive diagnosis. Evaluating response of bone sarcoma to initial chemotherapy by imaging methods is a challenge. Even with large necrotic area inside the tumor bulk, the tumor may not shrink significantly. This is due to the extensive osteoid and bony matrix which will remain static after chemotherapy [10]. At present, the gold standard for assessing the effects of chemotherapy is still histological examination of the resected tumor [6] [11] [12] [13]. Response is considered favorable if there is at least 90% tumor cell necrosis [14]. The degree of response is an important prognostic factor that can be used to plan post-surgical treatment and to optimize the timing of surgery [6] [7] [14] [15].

DCE-MR of osteogenic sarcoma had been performed and validated against

histological analyses of en bloc resections following initial chemotherapy. The results of these studies had demonstrated accuracies of approximately 90% for discrimination of response [16] [17] [18] [19] [20]. One study showed DCE-MR was a prognostic factor for event-free survival and overall survival before treatment, and was indicative of histologic response to neoadjuvant therapy [21]. In the assessment of the percentile of necrosis and thus the degree of response to the chemotherapy in our follow up scans, all of our cases correlated well with the pathology findings. Our findings in osteogenic sarcoma were comparable with the other studies.

We demonstrated that all benign tumors showed type 1 curves and all of their maximal enhancement signals (SI_{max}) were less than 350. Though limited in number, the cases in our study showed that the negative predictive value of type 1 curve for malignant tumor was 100%. It is therefore tempting to suggest that type 1 curve together with $SI_{max} < 350$ may be reliable indicators to differentiate benign from malignant tumors in pre-treatment cases. This is particularly useful for the planning of operation.

However, there were limitations in our study. Our sample size and characteristics of the samples were small. Our samples were a mixture of different tumors. The number of paired pre and post-treatment patients were small and limited. A larger sample size is desirable to further confirm our findings and to improve statistical power. In one case of intra-abdominal carcinoma of pancreas, type 2 curve was found. We considered that the TIC for this kind of tumor was not specific. DCE-MR might not be useful in this kind of intra-abdominal tumor. In one case of arm pPNET tumor, the presence of axillary lymph node impaired the blood flow, thus affecting our accuracy.

5. Conclusion

Despite small sample size, our results were very encouraging. In routine clinical practice, our study showed that DEC-MR might be useful in the differentiation of benign and malignant extra-cranial solid tumor in children and young adults. Based on our findings, type 1 curve with SI_{max} less than 350 is suggested as an additional indicator to assist in the differentiation of benign tumors in pre-treatment cases. We also think that DEC-MR may have a possible role in the monitoring of treatment response in extra-cranial childhood solid tumors. The lack of irradiation has an advantage over CT or PET in pediatric applications. However, a larger study is needed to further confirm our findings.

Conflicts of Interest

The authors declare no conflicts of interest regarding the publication of this paper.

References

[1] Kuhl, C.K., Mielcareck, P., Klaschik, S., Leutner, C., Wardelmann, E., Gieseke, J., *et*

al. (1999) Dynamic Breast MR Imaging: Are Signal Intensity Time Course Data Useful for Differential Diagnosis of Enhancing Lesions? *Radiology*, **211**, 101-110. https://doi.org/10.1148/radiology.211.1.r99ap38101

[2] Padhani, A.R. (1999) Dynamic Contrast-Enhanced MRI Studies in Human Tumours. *British Journal of Ophthalmology*, **72**, 427-431. https://doi.org/10.1259/bjr.72.857.10505003

[3] Nielsen, T., Wittenborn, T. and Horsman, M.R. (2012) Dynamic Contrast-Enhanced Magnetic Resonance Imaging (DCE-MRI) in Preclinical Studies of Antivascular Treatments. *Pharmaceutics*, **4**, 563-589. https://doi.org/10.3390/pharmaceutics4040563

[4] Weidner, N. (1996) Intratumoural Vascularity as a Prognostic Factor in Cancers of the Urogenital Tract. *European Journal of Cancer*, **32**, 2506-2512. https://doi.org/10.1016/S0959-8049(96)00378-4

[5] Bhujwalla, Z.M., Artemov, D. and Glockner, J. (1999) Tumor Angiogenesis, Vascularization, and Contrast-Enhanced Magnetic Resonance Imaging. *Topics in Magnetic Resonance Imaging*, **10**, 92-103. https://doi.org/10.1097/00002142-199904000-00002

[6] Raymond, A.K., Chawla, S.P., Carrasco, C.H., Fanning, C.V., Grice, B., Armen, T., *et al.* (1987) Osteosarcoma Chemotherapy Effect: A Prognostic Factor. *Seminars in Diagnostic Pathology*, **4**, 212-236.

[7] Glasser, D.B., Lane, J.M., Huvos, A.G., Marcove, R.C. and Rosen, G. (1982) Survival, Prognosis, and Therapeutic Response in Osteogenic Sarcoma. *Cancer*, **69**, 698-708. https://doi.org/10.1002/1097-0142(19920201)69:3<698::AID-CNCR2820690317>3.0.CO;2-G

[8] Verma, S., Turkbey, B., Muradyan, N., Rajesh, A., Cornud, F., Haider, M.A., *et al.* (2012) Overview of Dynamic Contrast-Enhanced MRI in Prostate Cancer Diagnosis and Management. *AJR*, **198**, 1277-1288. https://doi.org/10.2214/AJR.12.8510

[9] MacVicar, A.D., Olliff, J.F., Pringle, J., Pinkerton, C.R. and Husband, J.E. (1992) Ewing Sarcoma: MR Imaging of Chemotherapy Induced Changes with Histologic Correlation. *Radiology*, **184**, 859-864. https://doi.org/10.1148/radiology.184.3.1509080

[10] Senger, D.R., Galli, S.J., Dvorak, A.M., Perruzzi, C.A., Harvey, V.S. and Dvorak, H.F. (1983) Tumor Cells Secrete a Vascular Permeability Factor That Promotes Accumulation of Ascites Fluid. *Science*, **219**, 983-985. https://doi.org/10.1126/science.6823562

[11] Huvos, A.G. (1986) Osteogenic Sarcoma of Bones and Soft Tissues in Older Persons. A Clinicopathologic Analysis of 117 Patients Older than 60 Years. *Cancer*, **57**, 1442-1449. https://doi.org/10.1002/1097-0142(19860401)57:7<1442::AID-CNCR2820570734>3.0.CO;2-3

[12] Salzer-Kuntschik, M., Delling, G., Beron, G. and Sigmund, R. (1983) Morphological Grades of Regression in Osteosarcoma after Polychemotherapy—Study COSS 80. *Journal of Cancer Research and Clinical Oncology*, **106**, 21-24. https://doi.org/10.1007/BF00625047

[13] Picci, P., Bacci, G., Campanacci, D., Gasparini, M., Pilotti, S., Cerasoli, S., *et al.* (1985) Histologic Evaluation of Necrosis in Osteosarcoma Induced by Chemotherapy: Regional Mapping of Viable and Nonviable Tumor. *Cancer*, **56**, 1515-1521. https://doi.org/10.1002/1097-0142(19851001)56:7<1515::AID-CNCR2820560707>3.0.CO;2-6

[14] Rosen, G., Caparros, B., Huvos, A.G., Kosloff, C., Nirenberg, A., Cacavio, A., *et al.* (1982) Preoperative Chemotherapy for Osteogenic Sarcoma: Selection of Postoperative Adjuvant Chemotherapy Based on the Response of the Primary Tumor to Preoperative Chemotherapy. *Cancer*, **49**, 1221-1230. https://doi.org/10.1002/1097-0142(19820315)49:6<1221::AID-CNCR2820490625>3.0.CO;2-E

[15] Hudson, M., Jaffe, M., Jaffe, N., Ayala, A., Raymond, A.K., Carrasco, H., *et al.* (1990) Pediatric Osteosarcoma: Therapeutic Strategies, Results, and Prognosprognostic Factors Derived from a 10-Year Experience. *Journal of Clinical Oncology*, **8**, 1988-1997. https://doi.org/10.1200/JCO.1990.8.12.1988

[16] Erlemann, R., Reiser, M.F., Peters, P.E., Vasallo, P., Nommensen, B., Kusnierz-Glaz, C.R., *et al.* (1989) Musculoskeletal Neoplasms: Static and Dynamic Gd-DTPA-Enhanced MR Imaging. *Radiology*, **171**, 767-773. https://doi.org/10.1148/radiology.171.3.2717749

[17] Fletcher, B.D. (1991) Response of Osteosarcoma and Ewing Sarcoma to Chemotherapy: Imaging Evaluation. *AJR*, **157**, 825-833. https://doi.org/10.2214/ajr.157.4.1892044

[18] Bonnerot, V., Charpentier, A., Frouin, F., Kalifa, C., Vanel, D. and Di Paola, R. (1992) Factor Analysis of Dynamic Magnetic Resonance Imaging in Predicting the Response of Osteosarcoma to Chemotherapy. *Investigative Radiology*, **27**, 847-855. https://doi.org/10.1097/00004424-199210000-00016

[19] Reddick, W.E., Langston, J.W., Meyer, W.H., Gronemeyer, S.A., Steen, R.G., Chen, G., *et al.* (1994) Discrete Signal Processing of Dynamic Contrast-Enhanced MR Imaging: Statistical Validation and Preliminary Clinical Application. *Journal of Magnetic Resonance Imaging*, **4**,397-404. https://doi.org/10.1002/jmri.1880040327

[20] Reddick, W.E., Bhargava, R., Taylor, J.S., Meyer, W.H. and Fletcher, B.D. (1996) Dynamic Contrast-Enhanced MR Imaging Evaluation of Osteosarcoma Response to Neoadjuvant Chemotherapy. *Journal of Magnetic Resonance Imaging*, **5**, 689-694. https://doi.org/10.1002/jmri.1880050612

[21] Guo, J., Reddick, W.E., Glass, J.O., Ji, Q., Billups, C.A., Wu, J., *et al.* (2012) Dynamic Contrast-Enhanced Magnetic Resonance Imaging as a Prognostic Factor in Predicting Event-Free and Overall Survival for Pediatric Patients with Osteosarcoma. *Cancer*, **118**, 3776-3785. https://doi.org/10.1002/cncr.26701